chemosensors

MDPI

Article

Nanoplasmonic Biosensing Approach for Endotoxin Detection in Pharmaceutical Field

Adriano Colombelli [1,*], Elisabetta Primiceri [2], Silvia Rizzato [2,3], Anna Grazia Monteduro [2,3], Giuseppe Maruccio [2,3], Roberto Rella [1] and Maria Grazia Manera [1,*]

[1] CNR-IMM, Institute for Microelectronic and Microsystems, Campus Ecotekne, Via per Monteroni, 73100 Lecce, Italy; roberto.rella@cnr.it
[2] CNR-Nanotec Institute, Campus Ecotekne, Via per Monteroni, 73100 Lecce, Italy; elisabetta.primiceri@cnr.it (E.P.); silvia.rizzato@unisalento.it (S.R.); annagrazia.monteduro@unisalento.it (A.G.M.); giuseppe.maruccio@unisalento.it (G.M.)
[3] Department of Mathematics and Physics, University of Salento, 73100 Lecce, Italy
* Correspondence: adriano.colombelli@le.imm.cnr.it (A.C.); mariagrazia.manera@cnr.it (M.G.M.)

Abstract: The outer membrane of Gram-negative bacteria contains bacterial endotoxins known as Lipopolysaccharides (LPS). Owing to the strong immune responses induced in humans and animals, these large molecules have a strong toxic effect that can cause severe fever, hypotension, shock, and death. Endotoxins are often present in the environment and medical implants and represent undesirable contaminations of pharmaceutical preparations and medical devices. To overcome the limitations of the standard technique, novel methods for early and sensitive detection of LPS will be of crucial importance. In this work, an interesting approach for the sensitive detection of LPS has been realized by exploiting optical features of nanoplasmonic transducers supporting Localized Surface Plasmon Resonances (LSPRs). Ordered arrays of gold nano-prisms and nano-disks have been realized by nanospheres lithography. The realized transducers have been integrated into a simple and miniaturized lab-on-a-chip (LOC) platform and functionalized with specific antibodies as sensing elements for the detection of LPS. Interactions of specific antibodies anchored on protein A-modified sensor chips with the investigated analyte resulted in a spectral shift in the plasmonic resonance peak of the transducers. A good linear relationship between peak shifts and the LPS concentration has been demonstrated for the fabricated nano-structures with a detection limit down to 5 ng/mL. Integration with a proper microfluidic platform demonstrates the possibility of yielding a prototypal compact device to be used as an analytical test for quality determination of pharmaceutical products.

Keywords: nanoplasmonics; LSPR; lipopolysaccharides (LPS), gold nano-disks; biosensors

Citation: Colombelli, A.; Primiceri, E.; Rizzato, S.; Monteduro, A.G.; Maruccio, G.; Rella, R.; Manera, M.G. Nanoplasmonic Biosensing Approach for Endotoxin Detection in Pharmaceutical Field. *Chemosensors* **2021**, *9*, 10. https://doi.org/chemosensors9010010

Received: 19 November 2020
Accepted: 27 December 2020
Published: 4 January 2021

1. Introduction

Bacterial endotoxins are the most common and dangerous contaminants found in the finished pharmaceutical preparations and medical devices, which is why Pharmacopoeias strictly regulate its content limits.

The outer membrane of Gram-negative bacteria contains a series of bacterial endotoxins known as Lipopolysaccharides (LPS); each cell can contain over two million copies [1]. Their function is to screen off damaging compounds, while letting nutrients pass. Their release into the surrounding medium mainly happens during cell growth and division as well as during cell death.

These large molecules consist of a hydrophobic domain (lipid A), oligosaccharide core, and a polysaccharide domain known as O-antigen that is responsible for their toxic effect due to the strong immune responses induced in humans and animals. Endotoxins may be introduced into the bloodstream through contaminated intravenous devices or medications. The release of such pyrogenic compounds may lead to a rapid inflammation reaction resulting in fever, inflammation, endotoxemia, and septic shock followed in some

cases by organ failure and eventual death [2]. Actually, different bacterial species produce different types of LPS being able to evoke stronger or weaker human blood responses [3]. The amount of LPS present depends on the amount and identity of the bacteria or on the treatment the bacteria have undergone during production. For E. coli, an amount between 2 and 50 femtograms of LPS has been experimentally determined [4].

As they are resistant to conventional sterilization procedures, the endotoxins test constitutes one of the main tests in the quality control for the production of drugs, in the production process of sterile products, medical devices, and pharmaceutical products that have to be injected or implanted into the body. A lethal dose of intravenously injected LPS can be as low as 1 to 2 micrograms [5].

According to the European Pharmacopoeia [6], the limit of endotoxins being tolerated in parenterally administered substances is 5 endotoxin units (EU) per kg body mass (1 EU $\approx$ 100 pM) [7]. This specification leads to a maximum tolerable endotoxin amount of 350 EU per individual (based on a body mass of 70 kg) or a tolerance of 350 EU/mL for a parenteral product where a single dose would comprise 1 mL.

There are two main methods for endotoxin detection: the in vitro pyrogen test (IPT) and the test Limulus amebocyte lysate (LAL) [2]. The first method, the in vitro pyrogen test (IPT), as described in European Pharmacopoeia and United States Pharmacopeia (USP) [8], is based on the incubation of blood leukocytes with LPS that is a very potent inducer of endogenous pyrogen production. Then, after intravenous injection of the incubation supernatant, the induced fever curve in rabbits is monitored. Although still approved, it is now rarely used, owing to costs, being time consuming, and the absence of quantitative results, having been largely replaced by the LAL test. This second method is based on the endotoxin-stimulated coagulation of the amebocyte lysate obtained from horseshoe crabs [9]. Due to high sensitivity, it is today the standard method selected by the US, European, and Japanese Pharmacopoeias for endotoxin testing for parenteral drugs and medical devices (detection limit reported around 10^{-9} g/mL [10]). Despite their high sensitivity, they involve animals and are laborious, time consuming, and expensive. Yet, in LAL, as with most enzymatic tests, results are susceptible to changes in temperature and pH and to the presence of protease and/or impurities when applied to actual cell lysates. Moreover, although they have a high sensitivity in the pharmacy industry, there are limitations in demonstrating circulating LPS [11].

This present scenario demands novel techniques with new approaches for endotoxin detection. Demand for developing faster, accurate, and portable quality test platforms that do not require complicated and expensive assay steps is significantly challenging [12–17]. Such detection strategies can be combined with different bioreceptors, ranging from antibodies or transmembrane receptors [18] to aptamers [7,19] and peptides [12], from enzymes that have a high affinity for LPS to molecularly imprinted polymers [17,20]. Optical biosensors, uniquely when integrated with nanotechnology, can offer a qualified response for addressing these analytical needs, owing to the possibility of real-time analysis, label-free detection, and the small sample volume required. Among optical biosensors, localized surface plasmon resonance (LSPR)-based technologies are a powerful tool for high-sensitivity and label-free detection in a compact device setting. These optical transducers can easily be integrated inside miniaturized lab-on-chip (LOC) devices with a range of fluidic systems for analyte delivery, making them prominent routes for the realization of a portable sensor for an on-site diagnostic test or point-of-care devices [21].

In this work, we propose a sensitive biosensing approach exploiting optical and physicochemical properties of plasmonic nanostructures: their ability to concentrate light energy in nanoscale volumes, and subsequently, the increased near field intensity by several orders of magnitude with respect to incident light makes them a valuable transducing platform for endotoxin detection. In such nanostructures, a pivotal role in the sensing functionalities performance is played by electromagnetic field enhancement at the nanoscale, allowing probing interaction of biomolecules at the sensor surface. This is why they are ideal trans-

ducers for probing localized changes in a medium that allows a label-free method for detecting molecular interaction.

Developing techniques for tailoring the size and shape of the metal nanoparticles (NPs) and patterning them on a planar substrate in controlled spacing assemblies is a widely explored research ambit producing exciting results. Sensing functionalities are strictly related to the intensity and distribution of the probe electromagnetic fields; a proper choice of the sensing transducer geometry is a crucial point in the achievement of performant biosensor assay.

Different nanolithographies using colloidal particles as masks for etching or templates for the metal deposition are emerging as unconventional methods for the nano-fabrication of plasmonic structures on planar substrates. Varying the sizes and the arrangement of the colloids can systematically tune the dimensions, periodicity, and interspacing of the metal nanostructures and their corresponding plasmon resonances. The advantages of these techniques are mainly the versatility, low cost, and compatibility with wafer-scale processes as well as their potential to manufacture a broad selection of nanostructured materials.

Pioneering work by Van Duyne and co-workers reported the realization of a close-packed array (CPA) of polystyrene (PS) nanospheres self-assembled on a surface and characterized by a two-dimensional crystal-like structure with hexagonal geometry [22]. Planar distributions of long-range ordered array metal nano-prisms with tailored optical functionalities can be realized by depositing thin metals layers through the small apertures of the CPA.

An even easier method allows the self-assembly of electrostatically-driven charged colloids onto planar substrates, thus producing, with the same principle, short-range ordered arrays of metal nano-disks characterized by a more symmetric shape and tunable average interparticle distance but at the expense of array periodicity [23].

Upon interaction with visible light, electromagnetic field distribution is not uniform on different arrays, depending on the plasmonic nano-structure size, shape, spacing, and planar arrangement. Local intense areas of electromagnetic fields (EM) are expected to occur at sharp edges, nanoparticle gaps, and crevices, or other geometries with a sharp roughness. The different EM field distribution means a different ability in optically transducing biomolecular events at their surfaces.

In this work, we aim to compare sensing functionalities of long-range ordered Au nano-prisms and short-range ordered Au nano-disks arrays as transducing platforms for the sensitive detection of LPS in a liquid environment. The realized plasmonic transducers are integrated with a proper microfluidic platform in order to realize the prototype of a low-cost LOC biosensing platform intended for the detection of bacterial endotoxin to be used on a drug manufacturer site. Thus, a novel concept of the quality test is proposed, trying to exploit the advantages of the proposed techniques: reducing sample volume and data management and easy integration with information processing will be of great help for faster production and drug distribution.

2. Materials and Methods

2.1. Materials

Glass substrates (25 × 25 mm^2) were obtained from EOT Electro-Optical Technologies. Polystyrene (PS) spheres with a diameter of 80 nm, suitable for short-range order organizations, were purchased from Invitrogen and Polyscience Inc. Poly(diallyl dimethylammonium chloride) (PDDA, MW 200,000–350,000, Sigma-Aldrich, Darmstadt, Germany), Poly(sodium 4-styrene sulfonate) (PSS, MW 70,000, Sigma-Aldrich, Darmstadt, Germany) and Poly(allylamine hydrochloride) (PAH, MW 50,000, Sigma-Aldrich, Darmstadt, Germany) were purchased from Sigma-Aldrich. On the contrary, polystyrene nanospheres with a 500 nm diameter were purchased from Sigma-Aldrich in aqueous suspensions with a concentration of 10 wt%; the coefficient of variation (CV) was specified to be 2.4%, while the density of the PS particles is 1.05 g/cm^3.

Protein A, N-hydroxysuccinimide (NHS), N-(3-dimethylamino- propyl)-N0- ethylcarbodiimide hydrochloride (EDAC), and ethanolammine and 11-mercaptoundecanoicacid (11-MUA) were purchased from Sigma-Aldrich (Darmstadt, Germany). Anti- E. Coli Lipopolysaccharides (LPS) Antibody (Ig2b.k–Clone N.15j140), and Lipopolysaccharide from E. coli 0157:H7 were purchased from Abcam (Cambridge, United Kindom). Hybridization measurements were performed using a saline phosphate buffer (PBS, pH 7.4, Sigma-Aldrich, Darmstadt, Germany). Deionized water was used for the preparation of all solutions.

All experiments were carried out at a constant temperature of 24 °C, at humidity and temperature laboratory-controlled conditions.

2.2. Transducers Nanofabrication and Surface Functionalization

Plasmonic transducers nano-fabrication exploited the advantages of low-cost template-mediated techniques. Exploiting the advantages offered by top–down and bottom–up approaches, these methods provide an exciting alternative to sequential and costly fabrication techniques. The self-assembly of colloidal polystyrene nanoparticles by capillary and electrostatic interactions with planar substrates is the starting point of the procedure; we have tested both nano-fabrication routes.

In the first case, Nanosphere Lithography (NSL) enabled the fabrication of long-range order assemblies of Au nano-prisms on a glass substrate by depositing the metal through the apertures of an extremely cheap lithographic mask composed by a single and homogenous layer of polystyrene (PS) nanospheres. The PS nanospheres are self-assembled at the air/water interface in a homemade apparatus schematically described in [23].

The fabrication setup enables dispensing the particle suspension on a tilted glass slide with a controllable rate of release. A high-quality colloidal mask can only be obtained with substrates presenting a homogeneous hydrophilic surface. To achieve this condition, a pre-cleaning treatment was performed by ultrasonication with acetone, ethanol, and deionized water. Then, a well-established hydrophilization process based on oxygen plasma treatment (Diener Atto, 1 mbar O_2, 100 W, 5 min) has to be applied immediately before the deposition procedure. Furthermore, a 1:1 mixture of alcohol and polystyrene water solution was prepared to facilitate the trapping of polystyrene nanospheres at the air–liquid interface. A motorized syringe pump allows slowly dispensing a controlled volume of the colloidal solution onto the glass slide, enabling the CPA formation at the air/water interface. A two-step water removal realizes the transfer from the air–water interface to a solid substrate. This procedure allows avoiding possible monolayer damages by using a peristaltic pump and a self-vaporization step. After realizing the CPA, this approach allows the fabrication of nanostructured materials on the desired substrate by depositing metals through the small openings of a low-cost lithographic mask; further details can be found in Colombelli et al. [23]. In this work, the assembled monolayers have been exploited to realize the highly ordered array of a gold nano-prism characterized by a triangular shape. A physical deposition technique based on Electron Beam Evaporation (EBE) was adopted for the nano-structures fabrication. In particular, an ordered array of Au nano-prisms characterized by a triangular shape has been fabricated by depositing on the mask a layer of gold with a thickness of 40 nm. To improve the adhesion of Au structures on the glass substrate, a 2 nm thick Titanium layer was prepared. After the metal deposition, a mechanical lift-off process was performed to remove the colloidal mask revealing the fabricated nano-structures. A different fabrication strategy was developed for the realization of a short-range ordered array of colloidal nanospheres. The substrate is washed with acetone and isopropanol and then functionalized with polyelectrolytes layers by the layer-by-layer technique. In this way, negatively charged PS particles interact with the positively charged surface in order to facilitate particle absorption by electrostatic interactions as reported in our previous work [24]: the substrates were coated with of 0.1 wt% PDDA, followed by 0.1 wt% PSS and 0.1 wt% PDDA again by alternately dipping into the respective solutions for 5 min. Then, the polystyrene spheres were assembled by

immersing the functionalized substrates into the 0.2% nanospheres suspension in 2 mM solution of NaCl. After the optimized deposition of the PS particles, the samples were rinsed in boiling milli-Q water for 60 s to eliminate the excess of particles, rinsed again with milli-Q water at room temperature, and carefully dried in a nitrogen flow.

Successively, the realization of the gold nano-disk lattices is realized by Argon Reactive Ion Etching for 6 min to selectively remove the portion of the gold film not protected by the nanospheres. Finally, an oxygen plasma treatment was applied for 60 s in order to remove any nanosphere residues, thus revealing on the substrate the fabricated nano-structures.

Before the functionalization step, metal transducers were washed in a boiling solution of H_2O_2 (30%), NH_3 (30%), and milliQ water in a 1:1:5 ratio for 10 min and then rinsed with milliQ water. First, they were cleaned by O_2 plasma for 3 min and then immersed in an ethanol solution in order to remove eventual organic residues. A self-assembled 11-mercaptoundecanoic acid (11-MUA) layer on the Au nanostructures surface was prepared by submerging the transducers into a glycerol/ethanol (1:1, *v/v*) solution containing 150 mM 11-MUA for at least 12 h. For chemical binding between the 11-MUA adsorbed on Au and free amine of protein A, the carboxylic group of 11-MUA was activated by submerging the Au substrate modified with 11-MUA into a solution of 50 mM NHS for 10 min followed by 30 mM EDAC solution. Then NHS/EDAC solution was sent into the test chamber in a recirculation for 30 min in water/ethanol (10/1, *v/v*). The self-assembled protein A layer was fabricated by the incubation of the activated Au substrate in a solution of 10 mg/L protein A in 10 mM in ultra pure water. Before the immobilization of antibody, the self-assembled protein A layer on the Au substrate was blocked by inactivating the residual carboxyl group of 11-MUA with 1 M ethanolamine.

Once protein A molecules were properly immobilized onto the Au substrate, a solution containing 6 mg/mL of LPS antibodies in PBS buffer was dropped onto the transducers surface. After 1 h of incubation, the surface was washed with PBS buffer and incubated for 20 min with PBS containing 0.1% Tween20, in order to provide antigen access to the binding site of antibody by the separation of clustered antibody molecules. PBS buffer washing was performed prior to dropping the LPS solution prepared in PBS at an increasing concentration. A final step of washing stopped the experiment at each probed analyte concentration.

2.3. Numerical Methods

Different numerical models based on Finite Element Method (FEM) have been developed to theoretically explore the optical response of the fabricated nano-structures. In particular, a hexagonal array of gold nano-prisms and planar distributions of gold nano-disks on glass substrates have been considered. Several vital parameters have been modified to obtain a deeper understanding of their optical and electrical properties when the LSPR conditions are satisfied.

Owing to the hexagonal symmetry of the Long-Range (LR) periodic array and the perpendicular excitation using a linearly polarized light, a 3D simulation characterized by the geometry reported in Figure 1 can be developed to reduce the computational cost of the problem significantly. The geometries adopted in this model are characterized by specific dimensions derived by considering a close-packed array of hexagonal distributed nanospheres with a diameter of 500 nm. Starting from the bottom of the computational domain reported in Figure 1, the first domain represents the glass substrate, on which the gold nano-prisms have been fabricated. As reported in Figure 1, a truncated pyramid characterized by a triangular shape and a thickness of 40 nm was chosen to simulate the nano-structures. The last domain at the top represents the external environment. With appropriate boundary conditions, the built geometry represents the unit cell of the analyzed system.

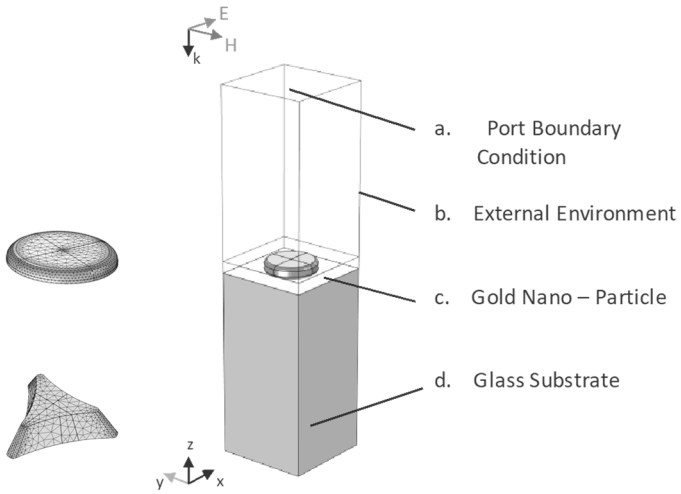

Figure 1. Schematic illustration of the model geometry used for the simulation of periodic array of Au nano-disks and nano-prisms on glass substrate; on the side, also the geometry and the mesh elements distribution of the simulated particles are reported.

On the contrary, the short-range (SR) ordered nano-disks have been simulated by considering the average inter-particles distance. Therefore, a homogeneous distribution of gold nano-disks can be approximated to a square periodic array of interacting particles. A 3D simulation characterized by the geometry reported in Figure 1 can be developed in this case, with a physical domain distribution similar to the one developed for LR ordered nano-structures. A cylinder characterized by a diameter of 80 nm and a thickness of 20 nm was chosen to simulate the metal structures.

A wavelength modulation technique was implemented in the model to investigate the optical response of these nanostructures. In particular, the LSPR generation was induced by simulating a polychromatic light beam coming from the top of the simulation domain. To calculate the reflection and transmission coefficients of the system, port boundary conditions were set for both the upper and lower faces of the simulation domain. Different boundary conditions were used on the unit cell's sides to simulate an infinite array of LR and SR ordered interacting plasmonic nano-structures characterized by hexagonal and square periodicity, respectively. The optical absorbance of single and periodic distributions of metal nano-structures characterized by different geometries can be predicted with the developed models, providing theoretical support to our experimental findings. In addition, the electric field distribution and the E/E0 field amplification were calculated to investigate the local field enhancement that arises near the particle surface when the resonance conditions are satisfied.

2.4. Optical Characterization

The optical characterization was conducted by performing absorption measurements in the UV-Visible (UV-VIS) spectral range by using a Cary500 UV-visible spectrophotometer (Varian Varian, Palo Alto, CA, USA). On the other hand, the plasmonic transducer characterization in transmission configuration and liquid phase was performed by using a compact optical fiber system equipped with a tungsten halogen light source (LS-1, wavelength range 360–2000 nm, Ocean Optics, Oxford, United Kindom), a portable spectrophotometer (USB2000 UV–Vis, wavelength ranging between 250 and 1100 nm, Ocean Optics, Oxford, United Kindom), and a couple of optical fiber probes (R-400-7 UV-VIS, Ocean Optics, Oxford, United Kindom). Polychromatic radiation emerging from the optical fiber was vertically focused onto the sample surface. Coupled with the detection fiber probe, the transmitted light was analyzed in a desired spectral range at room temperature using a portable UV-VIS spectrophotometer. The sensing response of the plasmonic transducers was investigated by following the spectral shift of the typical LSPR absorption peak in the

presence of liquid characterized by increasing refractive indices. Absorption measurements were performed in air (n = 1.00), water (n = 1.33), and different water/glycerol solutions. The presence of increasing glycerol concentrations enables exploring the transducers response in a selected range of refractive indices that goes from 1.33 (pure water) to 1.47 (pure glycerol).

2.5. Morphological Characterization

A Scanning electron microscope (Carl Zeiss SEM system) with an accelerating voltage of 5 kV was used to analyze the morphology and size of the realized nano-structures. SEM images have been acquired in top view configuration through an in-lens detector for secondary electrons. Image processing and analysis of particle distributions was performed by using ImageJ 1.42R (National Institutes of Health USA).

2.6. Integration of Plasmonic Biosensor into a Portable Lab-on-Chip Device

To develop a cost-effective, portable, and easy-to-use biosensing device, the fabricated nano-structures have been integrated on a miniaturized and straightforward lab-on-chip (LOC) platform. As a proof-of-concept, the LSPR platform operating in transmission configuration was developed, integrating the fabricated nano-structures into a suitable 2.5×2.5 cm^2 polydimethylsiloxane (PDMS) home-made microfluidic chip, which enables low-sample consumption and provide sensitivity and real-time response, raising the innovation in the design of biosensors as complete LOC device.

3. Results and Discussion

3.1. Morphology

Two different nanostructured plasmonic transducers have been fabricated exploiting different NSL-based techniques. The short-range ordered array of gold nano-disks reported in Figure 1a has been obtained using polystyrene particles with a diameter of 80 nm. The self-assembling of the colloidal mask can be tuned by controlling the electrostatic particle–surface or particle–particle interactions. The electrostatic interactions between negatively charged polystyrene nanospheres and a positively charged surface after layer-by-layer functionalization allow obtaining a homogenous colloidal distribution extended over a square centimeter scale. Nevertheless, the most significant effect is due to salt concentration solution that plays a crucial role in these interactions: it allows the control of not only interparticle electrostatic repulsion (and so the particle distance) but even particle–surface interactions. For these experiments, we have used a particle concentration of 0.2% and a NaCl concentration of 2 mM in solution resulting in excellent surface coverage (27%) and a low number of aggregates.

The average size of the Au nano-disks was about (80 ± 10) nm, while the average first neighbor distance was (50 ± 10) nm.

On the contrary, an ordered nano-prisms array was obtained by using as a mask a single layer of close-packed polystyrene nanosphere with an average diameter of 500 nm. This monolayer was realized by using a straightforward and highly reproducible bottom–up approach based on the self-assembling of the spheres at the air–liquid interface. After thermal evaporation of suitable gold thickness, the colloidal mask was removed, revealing on the substrate an array of gold nano-structures characterized by a triangular shape. The high magnification SEM image reported in Figure 2b shows a highly periodic distribution of metal nano-prisms characterized by a single oriented domain. The average size of the Au nanoparticles was about (127 ± 11) nm, referring to the length from an apex of the prism to its base, while the average first neighbor distance was (248 ± 12) nm.

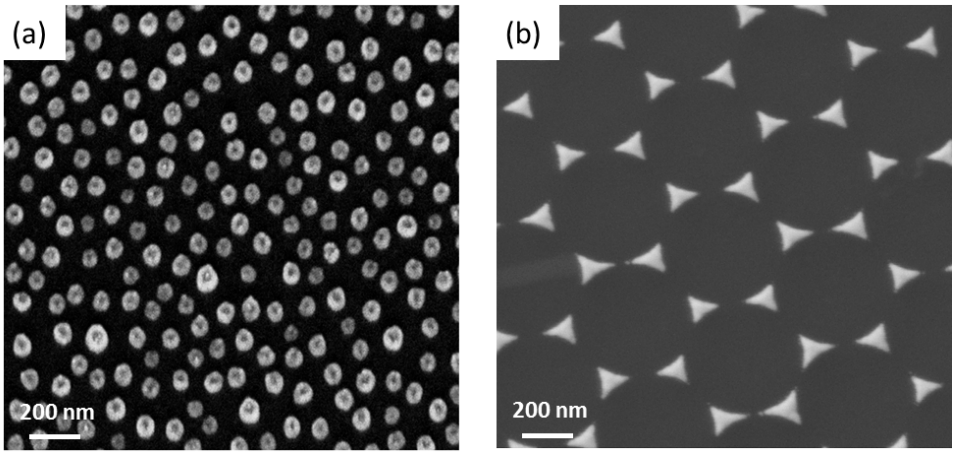

Figure 2. Top view SEM images of (**a**) gold nano-disks and (**b**) gold nano-prisms fabricated by NSL on glass substrate by using polystyrene (PS) nanospheres with diameters of 80 and 500 nm respectively.

3.2. Numerical Test

A periodic array of Au nano-prisms and nano-disks was theoretically analyzed. The activation of LSPR resonances was achieved using the wavelength modulation technique in transmission configuration. Owing to the localized surface plasmon resonance excitation, the normalized absorbance reported in Figure 3a exhibits a pronounced peak around λ = 654 nm for the short-range ordered array of a nano-disk and λ = 810 nm for the long-range ordered array of a nano-prism. The theoretical and experimental Absorbance spectra present similar optical features, exhibiting LSPR absorption peaks in the same spectral positions. All metal NPs have been considered homogeneous with the specific geometry reported in Figure 2. However, the optical response of the real sample could easily be affected by dimension or shape inhomogeneity. In addition, a numerical investigation on the electrical properties of the resonant metal NPs was developed. The Figure 3b shows the spatial distribution of the electric field enhancement E/E0 near the particle surface, when the LSPR conditions for dipole excitation are satisfied (λ = 654 nm for nano-disk and λ = 810 nm for nano-prism). As expected, the most considerable field enhancement can be generated on the edges of the NPs aligned with the incident light's polarization direction. Known in the literature as hot spots, these extremely localized and amplified electromagnetic fields attract much attention in designing sensors for bio-molecule detection. Indeed, metal nano-structures characterized by the presence of sharp tips can be optimized for molecular sensing providing higher sensitivity and resolution. In order to numerically investigate the sensing capabilities of the fabricated nano-structures, a comparison between their field enhancement E/E0 distribution in resonance condition is reported in Figure 3. As expected, the localized field intensity is much larger at the sharp edges of the triangular nano-prism. A field amplification of 70 was calculated near the gold nano-disks edges, while an enhancement factor of 125 was estimated for the nano-prism. This result can be attributed to higher electrons accumulation that can be achieved at the sharp edges of a nano-prism.

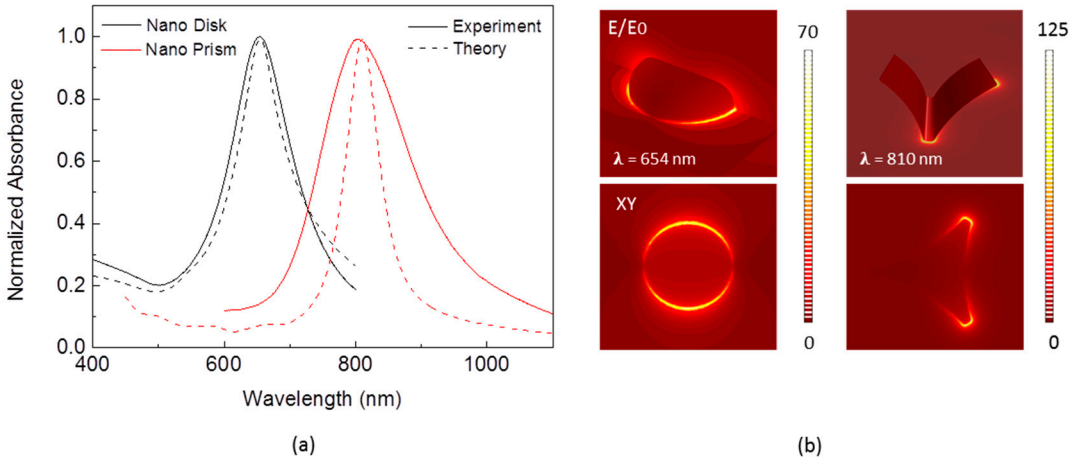

Figure 3. (**a**) Normalized absorbance spectra of disordered arrays of Au nano-disks fabricated by Nanosphere Lithography (NSL). The continuous lines are the experimental data, while the dashed lines are the calculated curves; (**b**) Electric Field Amplification (E/E0) distribution calculated for the fabricated NPs in resonance condition.

3.3. Optical Characterization

A Cary500 UV-visible spectrophotometer characterized the optical absorbance of the fabricated nano-structures in the Visible-near infrared (Vis-NIR) spectral range at room temperature. All the spectra were taken and compared with expected theoretical results calculated through numerical modeling. In particular, a comparison of the experimental and numerical normalized absorbance spectra of the fabricated nano-structures has been reported in Figure 3a.

The black curves describe the optical properties of a homogeneous distribution of gold nano-disks on glass substrates, with an average diameter of 80 nm. As expected from numerical modeling, upon excitation of the LSPR, the absorbance signal of the fabricated nano-structures exhibits a pronounced peak in the visible spectral range, with λ = 654 nm.

The red curves reported in Figure 3a describe the optical characterization of a periodic array of gold nano-prisms deposited on a glass substrate. The absorbance spectrum in the 600–1100 nm spectral range is shown and compared with the theoretical results obtained through numerical modeling. The signal obtained for the fabricated nano-structures exhibits a pronounced peak around λ = 810 nm, which can be attributed to the excitation of Localized Surface Plasmon Resonance of gold nano-prism. As can be noticed in Figure 3a, the spectral position of the experimental data results is very similar to the one theoretically calculated.

3.4. Refractometric Test

The sensing capabilities of the fabricated nano-structures have been theoretically and experimentally tested by monitoring their optical absorption in presence of an increasing refractive index of the external environment. The plasmonic transducers were exposed to several standard solutions prepared by glycerol diluted in deionized water. The optical response of the nano-structures was calibrated to specific refractive index (RI) variations in the range from 1.333 to 1.4. By submerging the systems in the prepared solutions, we monitored the variations of the LSPR absorption peak. As expected from numerical results, the effect of the high-index dielectric surrounding is a spectral shift of the resonance toward longer wavelengths, as can be noticed in Figure 4a, where the absorption spectra of Au nano-disks exposed to increasing glycerol concentrations have been reported. Similar results have been obtained with the hexagonal array of Au nano-prisms.

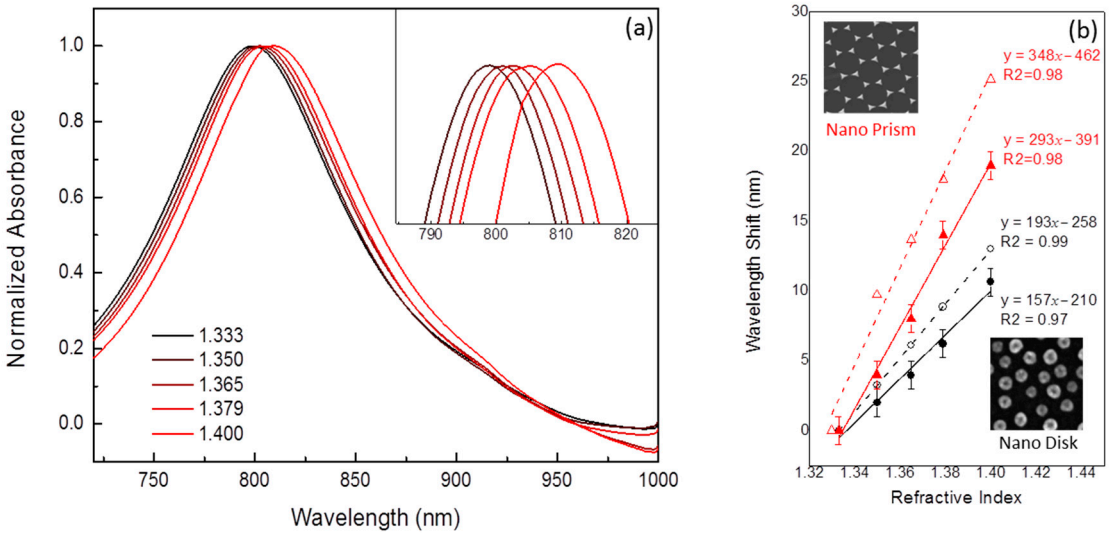

Figure 4. (**a**) Absorption spectra of Au nano-disks with an average diameter of 80 nm, exposed to different glycerol concentrations; the system was fabricated by NSL; (**b**) Comparison of the experimental and numerical calibration curves vs. a refractive index calculated for the fabricated system. In order to achieve statistically valid results, the average wavelength shift of five tests has been reported for each refractive index (RI) value. Trend-line equation and the R-square of each calibration curve are reported as well.

Figure 4b reports the corresponding numerical and experimental calibration curves calculated from the wavelength shift (nm) of the LSPR absorption peak in the presence of the different solutions. Wavelength peak shifts between two following RIs values are statistically different, while repeated measurements (n = 5) for each value have been carried out. As can be observed, the analyzed systems exhibit a linear dependence of LSPR response on the RI of the external environment, validating their ability to sense even slight variations in the refractive index. A bulk refractive index sensitivity of 157 nm/RIU was calculated for the nano-disks array from the slopes of the calibration curves. In comparison, a sensitivity of 293 nm/RIU was estimated for the periodic array of nano-prisms, thus demonstrating the possible exploitation of these very cheap plasmonic materials as opto-chemical sensors. The refractive index sensitivities obtained from the experiments are comparable with those calculated in our numerical models. Once again, we attribute the small differences between numerical and experimental results to the geometrical approximations adopted in the models. More specifically, in the case of SR ordered metal nano-disks array, even if the fabricated systems are characterized by different geometrical properties and spatial distribution, they present somewhat comparable sensing capabilities with higher sensitivity that can be obtained with a periodic array of metal nanoparticles. However, further optimization of the gold nano-disks density and size could actively improve the sensing performances of this kind of system.

3.5. Biosensors Evaluation

As proof of concept, an optical biosensor based on Localized Surface Plasmon Resonance has been developed for the sensitive detection of LPS. Long-range ordered and short-range ordered arrays of gold nano-structures of different sizes and shapes have been tested.

The functionalization process includes the overnight deposition of a mixed self-assembled monolayer (SAM) of mercaptoundecanoic acid (11-MUA) and activation of the carboxylic group with N-hydroxisuccinimide. The activated SAM can bind Protein A, which contains an Fc antibody-binding specific domain allowing an oriented immobilization of antibodies. As shown in Figure 5, each functionalization step was monitored by optical characterization by measuring the shift of the resonance peak in dry conditions. As an example, the typical absorption spectra of Au nano-prisms at each functionalization step are reported in Figure 5. As expected, each molecular layer onto the metal surface of the nano-prisms induces a redshift of the resonant LSPR peak, demonstrating a proper immobilization of the molecules onto the plasmonic transducer.

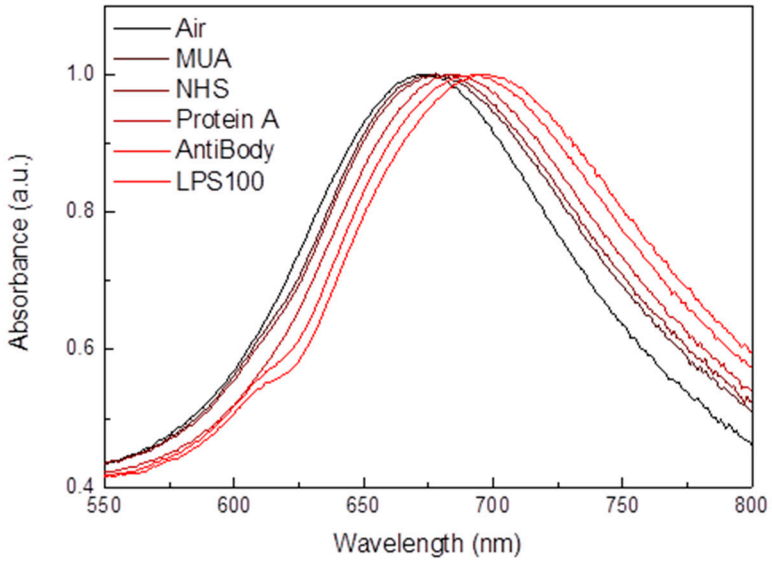

Figure 5. Normalized absorbance spectra of the short-range (SR) homogeneous distribution of Au nano-disks acquired during the biosensing measurements for the detection of Lipopolysaccharides (LPS) molecules. Absorbance spectra for each step of the functionalization process and also one LPS concentration are reported.

After antibodies immobilization, LPS molecules can be easily detected, allowing the evaluation of the sensor performances as a function of analyte concentration, as shown in Figure 6a. To this purpose, the functionalized nano-prisms were incubated with a solution of LPS in phosphate buffer saline (PBS) at different concentrations ranging from 5 to 100 ng/mL. A good linear relationship between sensors response and the LPS solutions at increasing concentrations has been demonstrated in the investigated concentration range for both nano-prisms and nano-disks array. An increased sensitivity (S) can be evidenced in the former with respect to the second arrangement. The limit of detection (LOD) of both transducing platforms can be calculated as LOD = $3\sigma/S$ [25,26], where σ represents the standard deviation of the measurand signal (taking into account resolution of the used instrumentation) resulting in 5 and 11 ng/mL for Au nanoprisms and nano-disks arrangements, respectively.

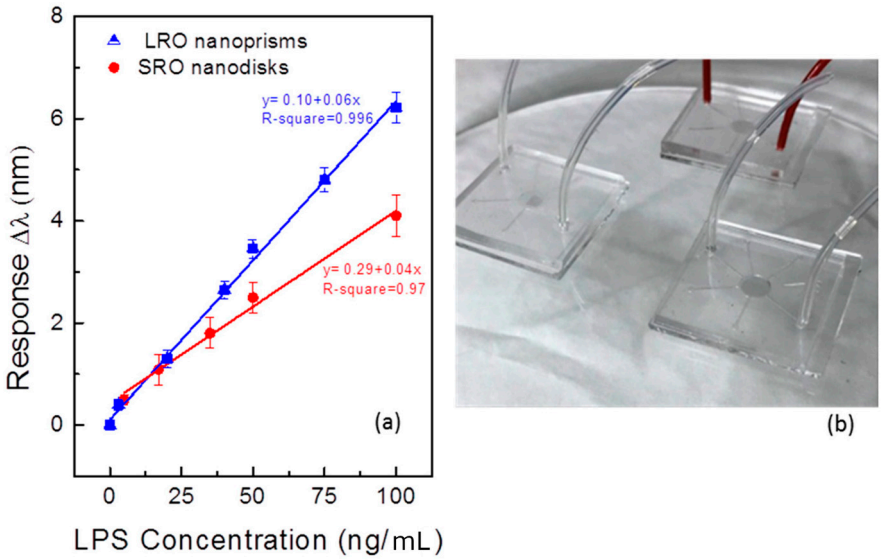

Figure 6. (**a**) Calibration curves of the functionalized plasmonic systems exposed to increasing concentrations of LPS. Trend line equations and R-square values are reported for each set of transducer. (**b**) Picture of the miniaturized lab-on-a-chip (LOC) platform based on the integration of nano-structured Localized Surface Plasmon Resonances (LSPR) transducers into a 2.5 × 2.5 cm^2 polydimethylsiloxane (PDMS) microfluidic chip.

Different sensing functionalities can be evidenced due to the different geometric arrangement as well as spatial distribution of the electromagnetic (EM) field obtained by the excitation of localized surface plasmon resonances. In particular, metal nanoprisms arrangements, characterized by a great EM field strictly localized at their sharp tips, results also in a large "sensing volume", which can be defined as the penetration depth within which changes of the refractive index can be detected. This is why a higher bulk sensitivity has been achieved with respect to metal nano-disks array both theoretically and experimentally (Figure 4). Such an SP-enhanced evanescent field is responsible also for the accurate quantification of analyte in a bare buffer solution, as in our experimental conditions. A large sensing volume could be detrimental in case of LPS detection in a complex matrix such as blood or serum, because of possible interference in the signal in the probing volume. So, in that case, further functional characterization will be needed. Despite this, the high concentration and localization of the electromagnetic field make them ideal probes for localized changes in a medium favoring also analyte detection by surface-enhanced spectroscopies. In the case of metal nano-disk arrangement, a more uniform distribution of the localized EM field has been evidenced on the metal surfaces, resulting in a more efficient investigation with traditional optical interrogation schemes (in transmission or reflection) easily integrated in miniaturized LOC platforms.

While a complete chemo-analytical biosensor characterization is outside of the aims of this work, an alternative transducing platform is proposed with respect to the conventional method. The reported results confirm that a promising tool for the sensitive and early identification of LPS in buffer solutions can be offered by exploiting tunable functional properties of plasmonic nanostructures properly arranged onto planar substrates. Low-cost nanofabrication methods are demonstrated to be able to follow this purpose.

4. Conclusions

In this work, an LSPR-based optical transducing platform has been realized and applied to detect bacterial endotoxins in buffer conditions. Different plasmonic transducers have been realized by nanospheres lithography: long-range ordered arrays of Au triangular nano-prisms and short-range ordered arrays of Au nano-disks have been fabricated, exploiting two different approaches for colloidal mask fabrication. Similar strategies enable us to avoid complicated and expensive fabrication facilities usually needed for

nano-fabrication. Theoretical and experimental optical characterization demonstrated a different distribution of the electromagnetic field on the nanostructures surfaces upon visible light excitation. The different optical near field behavior is responsible of different bulk sensitivities as demonstrated by functional characterization carried out by exposing them to different refractive index solutions. Specific antibodies have been chemically immobilized on the metal surfaces and used as sensing elements for the detection of LPS in buffer conditions. The sensor response (LSPR peak shift) as a function of LPS concentration has been tested, obtaining a linear relationship with a detection limit down to 5 ng/mL and around 11 ng/mL for nano-prisms and nano-disks, respectively.

Thus, a simple and practical transducing platform alternative to expensive and time-consuming conventional methods is proposed moving toward point-of-care diagnostics. Tunable optical and functional features dictated by geometrical aspects of the realized transducer can be obtained and oriented to the proper detecting strategies. While still being at a proof-of-concept stage, interesting volume and surface sensitivities are achieved, thus demonstrating the strong potential for endotoxins detection in real samples analysis such as injectable pharmaceutical preparations. Further miniaturization in the detection setup (by using LED as a light source and a complementary metal-oxide semiconductor CMOS as a detector for instance) can allow even integration with a smartphone.

Author Contributions: This manuscript was written through contributions of all authors. A.C. performed the NSL nanofabrication as well as spectral and sensing measurements with related statistical analysis and discussed optical properties of the long-range ordered systems writing the original draft paper; E.P. performed surface functionalization and biosensing assay tests contributing to original draft paper; S.R. prepared short-ordered nanostructures with relative discussion; A.G.M. prepared short-ordered nanostructures and performed morphological characterization with relative discussion; G.M. contributed to the discussion of data and supervised the nanofabrication and biosensing activities, R.R. and M.G.M. designed and discussed the whole experiments with a strong contribution in revision of the paper. All authors have read and agreed to the published version of the manuscript.

Funding: This research was funded by the project "Cluster in Bioimaging" (cod. QZYCUM0, "Aiuti a sostegno dei cluster tecnologici regionali 2014", Bando Regione Puglia n. 399 del 28/07/2014.

Data Availability Statement: The data presented in this study are available on request to the corresponding authors.

Acknowledgments: Authors are grateful to Enrico Melissano who performed the metal deposition in the clean room facilities and to Giovanni Montagna for technical support and LSPR optical set-up preparation.

Conflicts of Interest: The authors declare no conflict of interest.

References

1. Raetz, C.R.H. Biochemistry of endotoxins. *Annu. Rev. Biochem.* **1990**, *59*, 129–170. [CrossRef] [PubMed]
2. Raetz, C.R.H.; Whitfield, C. Lipopolysaccharide Endotoxins. *Annu. Rev. Biochem.* **2002**. [CrossRef] [PubMed]
3. Gnauck, A.; Lentle, R.G.; Kruger, M.C. Chasing a ghost? Issues with the determination of circulating levels of endotoxin in human blood. *Crit. Rev. Clin. Lab. Sci.* **2016**, *53*, 197–215. [CrossRef] [PubMed]
4. Watson, S.W.; Novitsky, T.J.; Quinby, H.L.; Valois, F.W. Determination of bacterial number and biomass in the marine environment. *Appl. Environ. Microbiol.* **1977**, *33*, 940–946. [CrossRef]
5. Sauter, C.; Wolfensberger, C. Interferon in human serum after injection of endotoxin. *Lancet* **1980**, *2*, 852–853. [CrossRef]
6. Available online: https://www.edqm.eu/en/european-pharmacopoeia-ph-eur-10th-edition (accessed on 19 November 2020).
7. Posha, B.; Nambiara, S.R.; Sandhyarani, N. Gold atomic cluster mediated electrochemical aptasensor for the detection of lipopolysaccharide. *Biosens. Bioelectron.* **2008**, *101*, 199–205. [CrossRef]
8. Available online: https://www.usp.org/ (accessed on 19 November 2020).
9. Duff, G.W.; Atkins, E. The detection of endotoxin by in vitro production of endogenous pyrogen: Comparison with limulus amebocyte lysate gelation. *J. Immunol. Methods* **1982**. [CrossRef]
10. Sakti, S.P.; Lucklum, R.; Hauptmann, P.; Bühling, F.; Ansorge, S. Disposable TSM-biosensor based on viscosity changes of the contacting medium. *Biosens. Bioelectron* **2001**, *16*, 1101–1108. [CrossRef]
11. Faraj, T.A.; McLaughlin, C.L.; Erridge, C. Host defenses against metabolic endotoxaemia and their impact on lipopolysaccharide detection. *Int. Rev. Immunol.* **2017**, *36*, 125–144. [CrossRef]

12. Zhang, J.; Khan, I.; Zhang, Q.; Liu, X.; Dostalek, J.; Liedberg, B.; Wang, Y. Lipopolysaccharides detection on a grating-coupled surface plasmon resonance smartphone biosensor. *Biosens. Bioelectron.* **2018**. [CrossRef]
13. Xu, W.; Tian, J.; Shao, X.; Zhu, L.; Huang, K.; Luo, Y. A rapid and visual aptasensor for Lipopolysaccharides detection based on the bulb-like triplex turn-on switch coupled with HCR-HRP nanostructures. *Biosens. Bioelectron.* **2017**. [CrossRef] [PubMed]
14. Brosel-Oliu, S.; Galyamin, D.; Abramova, N.; Muñoz-Pascual, F.X.; Bratov, A. Impedimetric label-free sensor for specific bacteria endotoxin detection by surface charge registration. *Electrochim. Acta* **2017**. [CrossRef]
15. Mayall, R.M.; Renaud-Young, M.; Chan, N.W.C.; Birss, V.I. An electrochemical lipopolysaccharide sensor based on an immobilized Toll-Like Receptor-4. *Biosens. Bioelectron.* **2017**. [CrossRef] [PubMed]
16. Rydosz, A.; Brzozowska, E.; Górska, S.; Wincza, K.; Gamian, A.; Gruszczynski, S. A broadband capacitive sensing method for label-free bacterial LPS detection. *Biosens. Bioelectron.* **2016**. [CrossRef] [PubMed]
17. Buchegger, P.; Lieberzeit, P.A.; Preininger, C. Thermo-nanoimprinted biomimetic probe for LPS and LTA immunosensing. *Anal. Chem.* **2014**. [CrossRef]
18. Yeo, T.Y.; Choi, J.S.; Lee, B.K.; Kim, B.S.; Yoon, H.I.; Lee, H.Y.; Cho, Y.W. Electrochemical endotoxin sensors based on TLR4/MD-2 complexes immobilized on gold electrodes. *Biosens. Bioelectron.* **2011**. [CrossRef]
19. Zhang, J.; Oueslati, R.; Cheng, C.; Zhao, L.; Chen, J.; Almeida, R.; Wu, J. Rapid, highly sensitive detection of Gram-negative bacteria with lipopolysaccharide based disposable aptasensor. *Biosens. Bioelectron.* **2018**. [CrossRef]
20. Altintas, Z.; Abdin, M.J.; Tothill, A.M.; Karim, K.; Tothill, I.E. Ultrasensitive detection of endotoxins using computationally designed nanoMIPs. *Anal. Chim. Acta* **2016**. [CrossRef]
21. Zandieh, M.; Hosseini, S.N.; Vossoughi, M.; Khatami, M.; Abbasian, S.; Moshaii, A. Label-free and simple detection of endotoxins using a sensitive LSPR biosensor based on silver nanocolumns. *Anal. Biochem.* **2018**. [CrossRef]
22. Camden, J.P.; Dieringer, J.A.; Zhao, J.; van Duyne, R.P. Controlled Plasmonic Nanostructures for Surface-Enhanced Spectroscopy and Sensing. *Acc. Chem. Res.* **2008**, *41*, 1653. [CrossRef]
23. Colombelli, A.; Lospinoso, D.; Taurino, A.; Manera, M.G. Tailoring a periodic metal nanoantenna array using low cost template-assisted lithography. *J. Mater. Chem. C* **2019**. [CrossRef]
24. Rizzato, S.; Primiceri, E.; Monteduro, A.G.; Colombelli, A.; Leo, A.; Manera, M.G.; Rella, R.; Maruccio, G. Interaction-tailored organization of large-area colloidal assemblies. *Beilstein J. Nanotechnol.* **2018**. [CrossRef] [PubMed]
25. Hastings, J.T. Optimizing Surface-Plasmon Resonance Sensors for Limit of Detection Based on a Cramer–Rao Bound. *IEEE Sens. J.* **2008**, *8*, 170–175. [CrossRef]
26. D'Amico, A.; di Natale, C. A contribution on some basic definitions of sensors properties. *IEEE Sens. J.* **2001**, *1*, 183–190. [CrossRef]